PERGAMON

International Journal of Solids and Structures 40 (2003) 2889–2904

INTERNATIONAL JOURNAL OF SOLIDS and STRUCTURES

www.elsevier.com/locate/ijsolstr

On the determination of the cohesive zone properties of an adhesive layer from the analysis of the wedge-peel test

T. Ferracin [a], C.M. Landis [b], F. Delannay [a], T. Pardoen [a,*]

[a] *Département des Sciences des Matériaux et des Procédés, Université catholique de Louvain, PCIM, Place Sainte Barbe 2, Louvain-la-Neuve B-1348, Belgium*

[b] *MEMS, MS 321Rice University, P.O. Box 1892, Houston, TX 77251, USA*

Received 25 November 2001; received in revised form 15 January 2003

Abstract

An extensive numerical study of the mechanics of the "wedge-peel test" is performed in order to analyze the mode I steady state debonding of a sandwich structure made of two thin plastically deforming metallic plates bonded with an adhesive. The constitutive response of the metallic plates is modeled by J_2 flow theory, and the behavior of the adhesive layer is represented with a cohesive zone model characterized by a maximum separation stress and the fracture energy. A steady-state finite element code accounting for finite rotation has been developed for the analysis of this problem. Calculations performed with the steady-state formulation are shown to be much faster than simulations involving both crack initiation and propagation within a standard, non-steady-state code. The goal of this study is to relate the measurable parameters of the test to the corresponding fracture process zone characteristics for a representative range of adherent properties and test conditions. An improved beam bending model for the energy release rate is assessed by comparison with the numerical results. Two procedures are proposed for identifying the cohesive zone parameters from experimental measurements.

Keywords: Adhesive bonding; Wedge-peel test; Cohesive zone; Steady-state FEM; Bond toughness

1. Introduction

Adhesive bonding of metallic plates has become a popular joining method in many industrial applications including the automotive, construction, microelectronics and aeronautics sectors. However, the development of the technique is hindered by several limitations as described by Cognard (2000). Among these limitations is the lack of reliable design criteria for adhesively bonded structures that account for failure of the joint. This problem is related to two issues. The first difficulty arises when attempting to *characterize the cracking resistance of adhesive bonds experimentally*. It is difficult to develop mechanical tests from which meaningful adhesive fracture properties can be extracted. An understanding of the intrinsic material

* Corresponding author. Tel.: +32-10-472417; fax: +32-10-474028.
E-mail address: pardoen@pcim.ucl.ac.be (T. Pardoen).

0020-7683/03/$ - see front matter © 2003 Elsevier Science Ltd. All rights reserved.
doi:10.1016/S0020-7683(03)00076-3

properties is needed to allow for the comparison of different adhesives and surface treatments. The second problem is related to the *prediction of failure* in bonded structures. Due to the wide range of constraints that can be induced by the substrates, depending on the geometry and loading configuration, the toughness of the joints has to be measured using a test adapted for the foreseen application. These difficulties have arisen due to the lack of adequate predictive fracture models that can assess the integrity of adhesive joints. For instance, linear elastic fracture mechanics leads to inaccurate predictions when plastic deformation occurs in the adherents. Moreover, all existing analytic non-linear fracture mechanics models also break down when the amount of plasticity within the adhesive bond is extensive.

The need for improved mechanical description of testing techniques, in particular when debonding is accompanied by plastic deformation of the adherents, is complemented by the need to develop models for the transfer of laboratory test results to the design of real structures. This study focuses on the first of theses two aspects of the problem with detailed analyses of the *wedge-peel test* using a *fracture process zone* to model the adhesive. Following previous investigations by Thouless et al. (1998) and Yang et al. (1999) based on a similar methodology, this work aims at relating the measurable parameters of the test to the corresponding fracture process zone characteristics for a representative range of adherent properties and test conditions.

In the wedge-peel test, two bonded metal plates are separated by means of a wedge inserted along the interface (Fig. 1). The wedge imposes a well-defined separation of the plates. If the plate thickness, h, is thin enough and the yield stress, σ_0, is small enough then plastic bending of the adherents occurs during the failure of the adhesive bond. Kim and Kim (1988) and Kim and Aravas (1988) have derived the relation between the bond toughness, Γ_0, and the critical values of these parameters that are needed to induce plastic bending during debonding:

$$\frac{\sigma_0}{E} \leqslant 3\frac{\Gamma_0}{\sigma_0 h} \tag{1}$$

where E is theYoung's modulus of the adherents.

In order to model the wedge-peel test, and to reduce the number of relevant fracture parameters, a so called "top-down" (Hutchinson and Evans, 2000) approach to fracture based on cohesive zone surfaces has

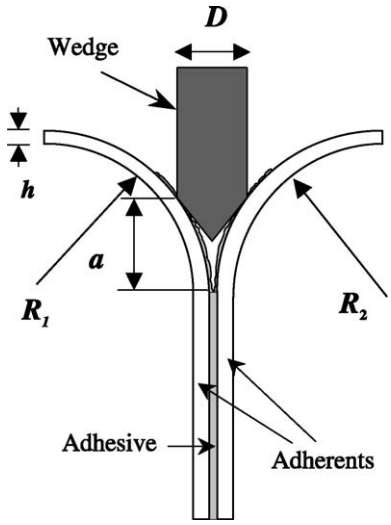

Fig. 1. Geometry of the wedge-peel test.

been adopted (Needleman, 1987; Tvergaard and Hutchinson, 1992). Applications of this approach to adhesive bonding have already been carried out for a number of problems (Tvergaard and Hutchinson, 1994, 1996; Yang et al., 1999; Mohammed and Liechti, 2000). Generally, these studies model the entire crack initiation and growth process within a standard finite element framework. In this work the cohesive zone is implemented within a steady-state finite element formulation (Dean and Hutchinson 1980; Wei and Hutchinson, 1997). This type of formulation is very efficient in terms of accuracy and speed, allowing for a systematic study of the influence of the parameters involved in the wedge-peel test. The relevant variables that will be investigated in this work are the mechanical properties of the substrate, the fracture process zone parameters describing the adhesive and the geometric characteristics of the test specimen.

In Section 2, the shape of the cohesive zone law is described. In Section 3, the steady-state FEM model is validated with a convergence study and by comparison with results obtained by similar simulations carried out on a non-steady-state commercial FEM code. A comprehensive study about the effects of the different test parameters on the resulting crack length and residual radius of curvature of the adherents is performed (no experimental result is presented in this paper). A simple beam bending model is also assessed through comparison with the FEM numerical method. Finally, two new calibration methods for identifying the cohesive zone parameters from experimental results are described.

2. Numerical model for steady state wedge-peel test

2.1. The interface traction-separation law

The entire adhesive layer is modeled as an interface traction-separation law that relates the normal traction on the crack plane, σ, to the interface opening displacement, δ. Since the entire adhesive layer is represented by the cohesive zone, both the failure process in the adhesive and the elasto-plastic deformation in the bulk of the adhesive are embodied in the traction-separation law as shown on Fig. 2.

The rate independent traction-separation law proposed by Tvergaard and Hutchinson (1992) with the form depicted on Fig. 2 has been chosen for this investigation. The two relevant quantities that characterize the fracture process zone are the peak stress σ_p and the area under the curve (Γ_0), which represents the fracture energy of the joint. As discussed by Tvergaard and Hutchinson (1992, 1994), the shape parameters

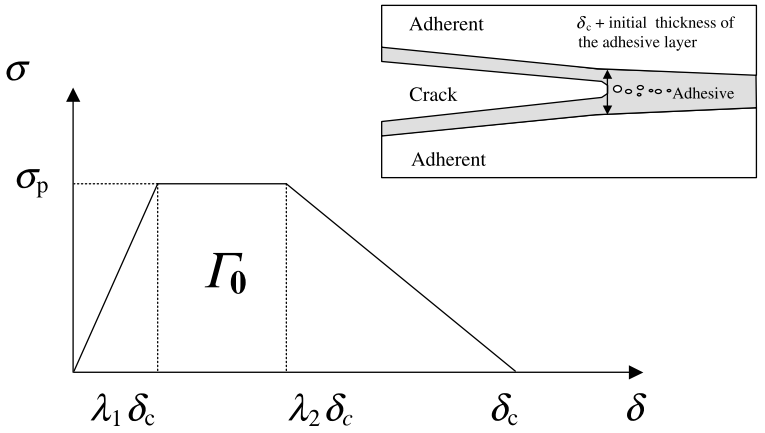

Fig. 2. The fracture process traction-separation law where δ_c is the maximum opening displacement, σ_p is the peak stress and λ_1 and λ_2 are shape parameters.

λ_1 and λ_2 are of secondary importance, and they will be taken to be equal to 0.15 and 0.5 for the remainder of this study. Note that once the maximum opening displacement δ_c, the peak stress σ_p, and the shape parameters λ_1 and λ_2 are chosen, Γ_0 can be obtained from

$$\Gamma_0 = \sigma_p \delta_c \left(1 - \frac{\lambda_1 + \lambda_2}{2}\right). \tag{2}$$

2.2. Model parameters

The adherents of thickness h are modeled using isotropic elastic-plastic, rate independent J_2 flow theory with uniaxial tension behavior given by

$$\sigma = \begin{cases} E\varepsilon & (\sigma \leqslant \sigma_0) \\ \dfrac{\sigma_0}{(\sigma_0/E)^n}\varepsilon^n & (\sigma > \sigma_0) \end{cases} \tag{3}$$

where E is the Young's modulus, σ_0 is the yield strength and n is the strain hardening exponent. The Poisson's ratio, v, is always taken equal to 0.3 in this study. The behavior of the adhesive layer is modeled by the traction-separation law presented in the previous subsection, and is characterized by Γ_0 and σ_p.

Within the finite element calculations, the radius of curvature of the plastically deformed adherents, R, is computed as illustrated in Fig. 3. The crack length is the distance between the crack tip (i.e. the position where the crack opening is equal to δ_c) and the wedge (i.e. the location of the applied displacement boundary condition).

The wedge-peel test system of Fig. 3 can be described by the following parameters: E, v, σ_0, n, h (adherent); Γ_0, σ_p (adhesive layer) and D (height of the wedge). Dimensional analysis leads to a normalization of the radius of curvature R and crack length a by the substrate thickness h. These quantities are likely to be measured during an experiment and are functions of the following dimensionless parameters

$$\frac{R}{h} = F_1\left\{\frac{\sigma_0}{E}, n, v, \frac{\Gamma_0}{\sigma_0 h}, \frac{\sigma_p}{\sigma_0}, \frac{D}{h}\right\}, \quad \frac{a}{h} = F_2\left\{\frac{\sigma_0}{E}, n, v, \frac{\Gamma_0}{\sigma_0 h}, \frac{\sigma_p}{\sigma_0}, \frac{D}{h}\right\}. \tag{4}$$

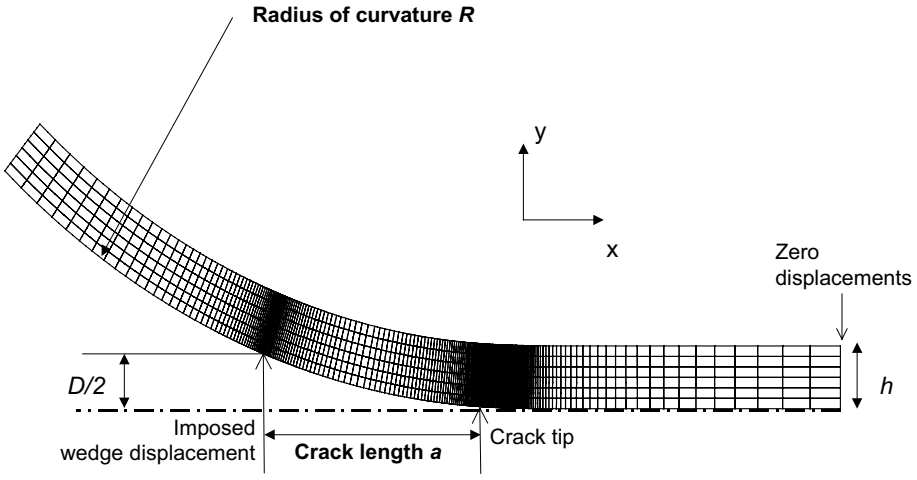

Fig. 3. FEM mesh used for modeling the wedge-peel test with the steady-state framework.

2.3. Numerical procedure

A linear kinematics finite element formulation for the study of steady state crack propagation in elasto-plastic materials was first applied by Dean and Hutchinson (1980) and later implemented by several other authors (e.g. Wei and Hutchinson, 1997). This formulation has also been applied to rate dependent fracture of epoxy by Landis et al. (2000). The steady state FE method is based on finding an equilibrium solution for the displacements based on a previous approximate distribution of plastic strains and then integrating the plasticity laws along streamlines to determine new approximations for stresses and plastic strains. This procedure is then repeated until convergence is achieved.

Unfortunately, for the analysis of the wedge-peel test the linear kinematics formulation is not sufficient. If we assume that the sliding between the wedge and the plates is frictionless, then, under steady state conditions, the critical energy release rate for the specimen is equal to the force per unit length required to push the wedge in the direction of crack propagation. If one attempts to analyze this problem with a linear kinematics formulation, then the force that the wedge applies to the plates can only be perpendicular to the crack extension plane and there is no driving force available for crack propagation. Hence, at the very minimum, the problem requires a large rotation formulation. The variational principle for such problems is written as follows

$$\int_V S_{ij}\delta\varepsilon_{ij}\,\mathrm{d}V = \int_S t_i\delta u_i\,\mathrm{d}S \tag{5}$$

where V is the volume of the body in the reference configuration, S is its surface, S_{ij} are the components of the second Piola–Kirckhoff stress tensor, t_i are the components of the traction vector applied to the boundary, u_i are the components of the total displacement vector, and ε_{ij} are the components of the Green–Lagrange strain tensor given in terms of displacement gradients as

$$\varepsilon_{ij} = \tfrac{1}{2}(u_{i,j} + u_{j,i} + u_{k,i}u_{k,j}). \tag{6}$$

The iterative procedure used to solve for the distribution of plastic strain is based on (5), and assumes *small strains* such that ε_{ij} can be additively decomposed into elastic and plastic parts. Then, the constitutive law for the second Piola–Kirckhoff stress is given as

$$S_{ij} = C_{ijkl}(\varepsilon_{kl} - \varepsilon^{\mathrm{p}}_{kl}) \tag{7}$$

where C_{ijkl} are the components of the elastic stiffness tensor that can be written in terms of E and v for isotropic materials, and $\varepsilon^{\mathrm{p}}_{ij}$ is the plastic part of the strain. Note that large rotations are accounted for. The plastic strains are determined by J_2 flow theory. Within a spherical yield surface given by $3S'_{ij}S'_{ij}/2 - \sigma_0^2 = 0$, where S'_{ij} is the deviatoric part of S_{ij}, the increments of plastic strain are zero. However, when the stress state is on the yield surface and the load increment is directed outward from the surface, plastic strains are given in incremental form as

$$\dot{\varepsilon}^{\mathrm{p}}_{ij} = \frac{3}{2}\dot{\bar{\varepsilon}}^{\mathrm{p}}\frac{S'_{ij}}{\overline{S}} \tag{8}$$

where $\overline{S} = (3/2S'_{ij}S'_{ij})^{1/2}$ is the effective stress, and $\dot{\bar{\varepsilon}}^{\mathrm{p}} = (2/3\dot{\varepsilon}^{\mathrm{p}}_{ij}\dot{\varepsilon}^{\mathrm{p}}_{ij})^{1/2}$ is the effective plastic strain increment. A power law hardening rule derived from Eq. (3) is used to relate the effective stress to the effective plastic strain as

$$\left(\frac{\overline{S}}{\sigma_0}\right)^{1/n} - \frac{\overline{S}}{\sigma_0} = \frac{E\bar{\varepsilon}^{\mathrm{p}}}{\sigma_0} \tag{9}$$

where $\bar{\varepsilon}^{\mathrm{p}} = \int \dot{\bar{\varepsilon}}^{\mathrm{p}}\,\mathrm{d}t$ is the accumulated effective plastic strain. In a manner analogous to decomposing the strain into elastic and plastic parts, the crack opening displacement is decomposed into a linear and a

non-linear part. The primary purpose of this decomposition is to facilitate the numerical computations. Hence the variation of the tensile stress t follows the cohesive surface constitutive law depicted in Fig. 2 as

$$T = \kappa(\delta - \delta^{\mathrm{p}}) \tag{10}$$

where κ is the initial slope of the traction-separation law and δ^{p} represents the non-linear or plastic part of the opening displacement. Note that δ^{p} must be carefully defined at each portion of the traction-separation curve since discontinuities in the slope exist, and furthermore, $\delta^{\mathrm{p}} = 0$ in the initial linear part of the curve.

The iterative procedure used to determine the distribution of plastic strains is analogous to that used for the linear kinematics formulation and is written as

$$\int_V \delta\varepsilon_{ij} C_{ijkl}\, {}^{n+1}\varepsilon_{kl}\, \mathrm{d}V + \int_{S_c} \delta u_1 \kappa\, {}^{n+1}\delta\, \mathrm{d}S = \int_V \delta\varepsilon_{ij} C_{ijkl}\, {}^{n}\varepsilon^{\mathrm{p}}_{kl}\, \mathrm{d}V + \int_{S_c} \delta u_1 \kappa\, {}^{n}\delta^{\mathrm{p}}\, \mathrm{d}S + \int_S t_i \delta u_i\, \mathrm{d}S. \tag{11}$$

Here ${}^{n+1}\varepsilon_{ij}$ and ${}^{n+1}\delta$ are the strain and crack opening displacement computed at the $n+1$th iteration and ${}^{n}\varepsilon^{\mathrm{p}}_{ij}$ and ${}^{n}\delta^{\mathrm{p}}$ are the plastic strain and plastic part of the crack opening displacement computed at the previous, i.e. the nth iteration. Then, V is the volume of the material in the reference configuration, S_c is the cohesive surface ahead of the crack tip, and S is the external surface in the reference configuration where tractions or displacements are applied. The integrals on the left side of Eq. (11) form the stiffness matrix and vector of unknown displacements at the $n+1$th iteration. The surface integrals over S_c account for the cohesive tractions ahead of the crack tip. The volume integral on the right hand side can be interpreted as a body force due to plastic strains. In order to alleviate convergence problems associated with the cohesive zone elements, an optimal lumping procedure (Gaudenzi and Bathe, 1995) was used to perform the cohesive surface integrations.

The solution procedure is described as follows. During a given step of the procedure the plastic strains are known from the previous step and *fixed*. Eq. (11) then defines a set of non-linear finite element equations that must be solved with a Newton–Raphson method. Let us call this the equilibrium iteration. Note again that during the equilibrium iterations the plastic strain distributions do not change. Once the equilibrium iterations have converged to a solution for the given distribution of plastic strains, a new plastic strain distribution is approximated by integrating the plasticity law, Eq. (8), along streamlines defined by a constant distance above or below the crack plane. Let us call this the plasticity iteration. Hence, for each plasticity iteration there are multiple equilibrium iterations. Then, the entire computation is complete when the distributions of plastic strains converge.

The FEM model for the wedge-peel test is illustrated in Fig. 3. Since the test is symmetric about the crack plane, only half of the specimen needs to be analyzed. Plane strain conditions are assumed as the width of the substrate is much larger than its thickness h and thus any three-dimensional effects such as anticlastic bending are neglected. The crack is assumed to have propagated a sufficient distance such that steady state conditions prevail for the entire structure. The wedge is modeled with a fixed displacement boundary condition of magnitude $D/2h$ above the plane of symmetry. Appropriate boundary conditions have been imposed on the right hand side of the structure as shown in Fig. 3 in order to prevent a rigid body motion. A mesh convergence study has been carried out to ensure accuracy. The mesh was particularly refined at the point of contact of the wedge and at the crack tip.

3. Numerical results of the steady state wedge-peel test model

3.1. Validation and comparison with standard finite element formulation

Prior to initiating the parametric study of the wedge-peel test, a mesh convergence analysis was performed. Results obtained using the mesh illustrated in Fig. 3, with refinement near the crack tip and at the

contact point of the wedge, were found to be in good agreement with convergent results from a uniformly refined mesh. As a final validation, results from the steady-state formulation were compared to simulations involving both crack initiation and growth performed with the non-steady-state FE program ABAQUS version 5.8 (1997), Ferracin et al. (2000). Results from the two methods for the radius of curvature of the deformed adherents were in agreement to within 10%. However, the steady state formulation was more than 20 times faster than the standard formulation facilitating the extensive parametric study of the wedge-peel test.

3.2. Results of the parametric study

The following results illustrate the dependence of the normalized crack length and radius of curvature on the dimensionless parameters appearing in Eq. (4). The results will be presented for realistic ranges of the parameters, i.e. for typical metal/adhesive bonds. The bond toughness $\Gamma_0/\sigma_0 h$ was chosen to range from 0.001 to 0.1. Normalized peak stress values, σ_p/σ_0, greater than 1.0 have not been studied due to the relatively low strength of adhesives in comparison to the metal adherents. Values of $\sigma_0/E = 0.001$, 0.003, 0.01 were investigated with 0.001 typical of low carbon steel or pure aluminum, and 0.01 the upper limit for structural hardened aluminum or martensitic steel. The hardening exponents, $n = 0$, 0.1, 0.2 are typical of structural alloys. The normalized wedge thickness D/h ranged from 0.45 to 5.0. Finally, the normalized radius of curvature will usually be displayed for values between 10 and 250.

Figs. 4 and 5 (a)–(c) show the variation of the crack length and the radius of curvature as a function of the normalized bond toughness $\Gamma_0/\sigma_0 h$, with $D/h = 1.5$ and various values of σ_p/σ_0, σ_0/E and n. As expected, both R/h and a/h decrease with increasing bond toughness $\Gamma_0/\sigma_0 h$. For very low bond toughness adhesives, i.e. when the condition of Eq. (1) is not satisfied, plastic bending of the adherents does not occur such that the results from linear elastic analysis of the wedge test apply. In this case, R/h tends to infinity and a/h tends to a finite value. Using elastic beam theory and a one parameter energy release rate fracture criterion, a/h is given by

$$\frac{a}{h} = \left[\frac{3}{16}\left(\frac{D}{h}\right)\left(\frac{\sigma_0 h}{\Gamma_0}\right)\left(\frac{E}{\sigma_0}\right)\right]^{1/4}. \tag{12}$$

The present model tends to match Eq. (12) for large σ_p/σ_0 and small $\Gamma_0/\sigma_0 h$ (Williams and Hadavinia, 2002). This result is expected since, as $\sigma_p/\sigma_0 \to \infty$ the cohesive zone fracture criterion approaches a single

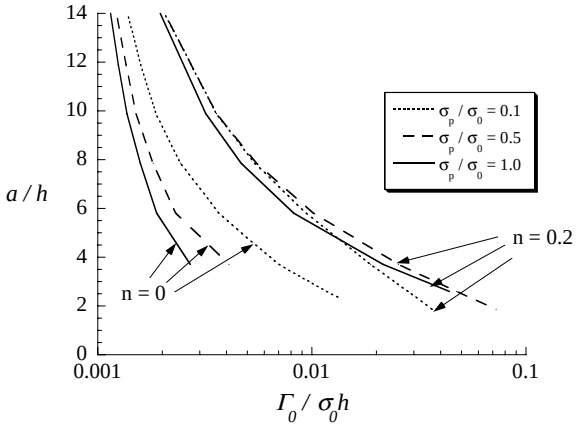

Fig. 4. Variation of the crack length as a function of the bond toughness for $\sigma_0/E = 0.001$ and $D/h = 1.5$.

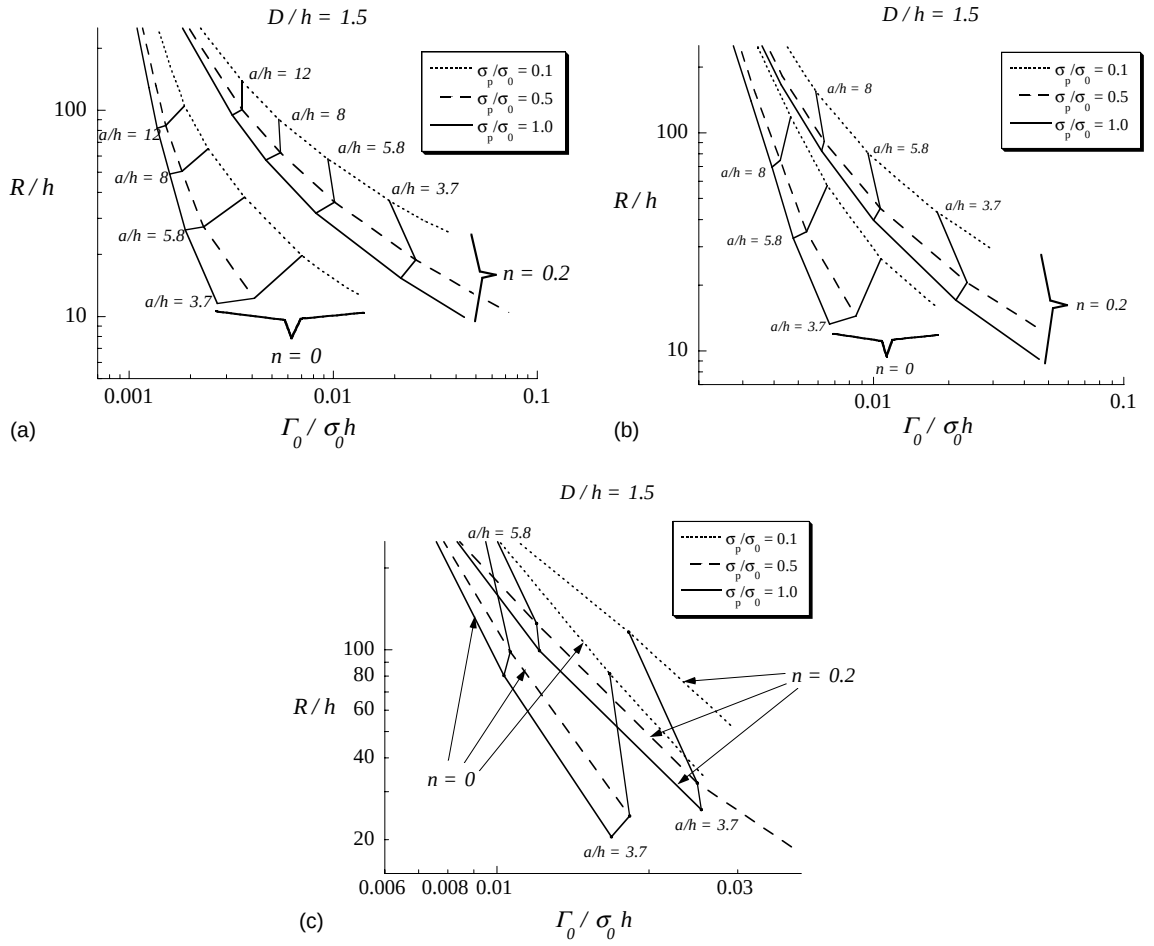

Fig. 5. (a) Variation of the radius of curvature and the crack length as a function of the bond toughness for $\sigma_0/E = 0.001$; the crack lengths are presented as constant crack length curves with their respective values a/h directly indicated in the figure. (b) Variation of the radius of curvature and the crack length as a function of the bond toughness for $\sigma_0/E = 0.003$; the crack lengths are presented as constant crack length curves with their respective values a/h directly indicated in the figure. (c) Variation of the radius of curvature and the crack length as a function of the bond toughness for $\sigma_0/E = 0.01$; the crack lengths are presented as constant crack length curves with their respective values a/h directly indicated in the figure.

parameter critical energy release rate criterion, and as $\Gamma_0/\sigma_0 h \to 0$ the plastic deformation in the adherents is negligible.

Fig. 5(a)–(c) show the variation of R/h with respect to $\Gamma_0/\sigma_0 h$ along with the corresponding values of a/h for two different hardening exponents. Note that less deformation is required to attain a given magnitude of stress as strain hardening increases. Hence, for a given value of the peak stress and bond toughness, the normalized radius and crack length increase as the strain hardening exponent n increases.

Notice on Figs. 4 and 5 that, for some values of the bond toughness, identical crack lengths result from two different peak stresses and two different states of specimen deformation. This phenomenon, that depends on n and σ_0/E, arises because lower peak stresses lead to cohesive tractions ahead of the crack tip that are distributed over a longer distance resulting in a longer *effective* crack length and therefore different deformations in the structure.

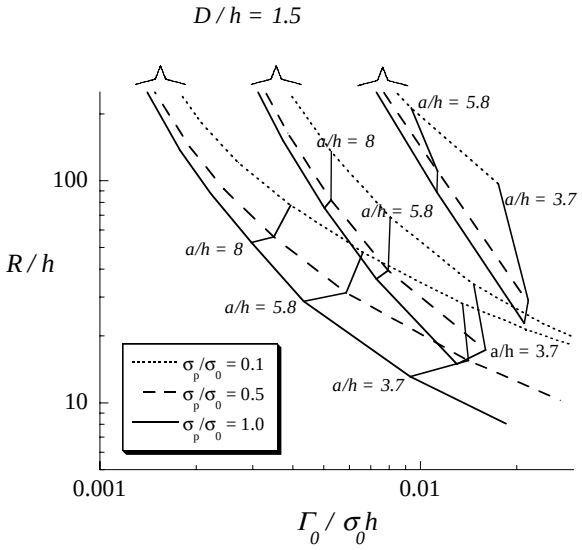

Fig. 6. Variation of the radius of curvature and the crack length as a function of the bond toughness with $\sigma_0/E = 0.01$, 0.003 and 0.001 and $n = 0.1$; the crack lengths are presented as constant crack length curves with their respective values a/h directly indicated in the figure.

Fig. 6 displays the effect of σ_0/E on R/h and a/h as a function of $\Gamma_0/\sigma_0 h$ for $n = 0.1$ and $D/h = 1.5$. For a given value of bond toughness, an increase of σ_0/E causes an increase of R/h. This is due to the elastic unloading which brings about an increase of the radius of curvature as a result of the decrease of the Young's modulus E. An increase of σ_0/E also causes an increase of the slope of these curves.

The effect of wedge thickness D/h on the relationship between the radius of curvature and crack length and the bond toughness is studied in Fig. 7 for $D/h = 0.45$ and 5.0 and $\sigma_0/E = 0.001$. For a given adhesive

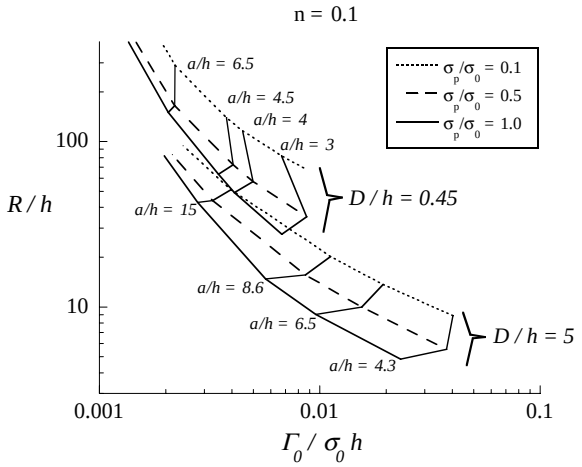

Fig. 7. Variation of the radius of curvature and the crack length as a function of the bond toughness for two values of the wedge thickness with $\sigma_0/E = 0.01$; the crack lengths are presented as constant crack length curves with their respective values a/h directly indicated in the figure.

and test specimen geometry, using a thicker wedge increases the crack length and diminishes the radius of curvature. Yang et al. (1999) have shown that, if the wedge is too small, the deformation of the arms will be dominated by shear rather than by bending, leading to a smaller curvature of the substrate (i.e. larger radius of curvature) for a given bond toughness, in agreement with our calculations. The beam bending theory, to be presented in the next section, which neglects these shear stresses will obviously not account for this dependence of the curvature on the wedge thickness.

4. Discussion

4.1. Comparison of the numerical simulations with a beam bending model

In this section, a beam bending solution including elastic unloading of the adherents is presented for the calculation of the bond toughness. The importance of the modeling of the elastic unloading is emphasized. The differences between this model and the FEM calculations are assessed and correction factors are derived.

By considering (i) steady state conditions, (ii) plastic beam theory and (iii) flow properties described by Eq. (3), Yang et al. (1999) derived the following relationship between the radius of curvature and the bond toughness,

$$\frac{\Gamma_0}{\sigma_0 h} = \left[\frac{8\alpha^3}{3(1-\nu^2)} - \frac{8\alpha}{n+2}\left(\frac{2\alpha}{\sqrt{3}}\right)^{n+1}\right]\left(\frac{\sigma_0}{E}\right)^2\frac{R}{h} - \left[\frac{\alpha}{1-\nu^2} - \frac{2}{n+1}\left(\frac{2\alpha}{\sqrt{3}}\right)^{n+1}\right]\left(\frac{\sigma_0}{E}\right) + \frac{2n}{(n+2)(n+1)}\left(\frac{h}{\sqrt{3}R}\right)^{n+1}\left(\frac{E}{\sigma_0}\right)^n \tag{13}$$

where $\alpha = (1-\nu^2)/(1-\nu+\nu^2)^{0.5}$.

Eq. (13) can be improved upon by taking into account the reduction of the radius of curvature due to elastic unloading experienced in the adherents once they are no longer in contact with the wedge. This effect can be evaluated as follows. Let the final radius of curvature of the adherents after debonding be R_f and the radius of curvature during debonding be R_d. The deformed beam experiences an elastic reversal ΔR_e during the drop to zero of the bending moment, M, induced at the crack tip by the wedge. If I is the moment of inertia of the metal adherent and E its Young's modulus, R_d can be evaluated using

$$\frac{1}{R_d} = \frac{1}{R_f} + \frac{1}{\Delta R_e} \tag{14}$$

with

$$\frac{1}{\Delta R_e} = \frac{M}{EI} = \frac{\int_0^h \sigma(z) z\,dz}{EI}. \tag{15}$$

An analytical solution of this problem in the elastic-perfectly-plastic case was given by Sener (1998). For power law strain hardening, Eq. (14) is solved iteratively by imposing R_f while ΔR_e is evaluated using (15). Selected results are shown in Fig. 8 for $\sigma_0/E = 0.001$ and 0.01 and $n = 0$ and 0.2. For $\sigma_0/E = 0.001$, the correction for elastic unloading is larger than 10% when R_f is larger than 30 times the substrate thickness. For $\sigma_0/E = 0.01$, i.e. in a high strength adherent, the correction is larger than 10% when R_f is only 3–4 times larger than the substrate thickness. Fig. 8 also shows very small dependence of the elastic unloading on the hardening coefficient n.

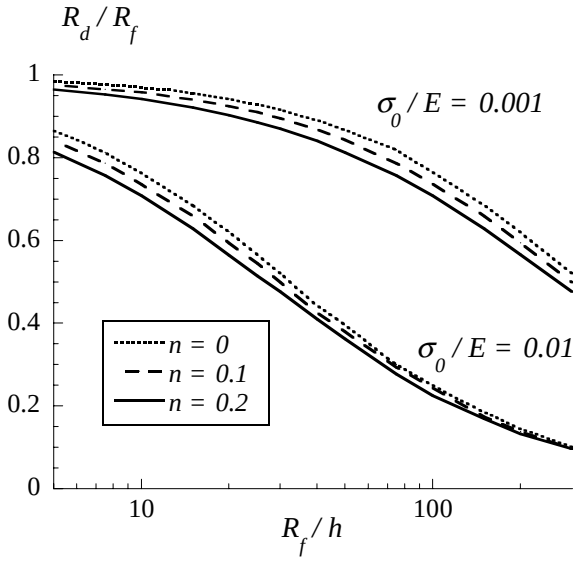

Fig. 8. Ratio of the initially applied radius of curvature and its final value after elastic unloading of the adherents evaluated using Eqs. (13) and (14).

A comparison is now made between the beam model accounting for the elastic unloading and the steady state FEM predictions. The differences in the results of the two models are due to the approximation of the beam bending in the first model, which neglects shearing, and to the fracture criteria used in the two models, which are a critical energy release rate for the beam model and a cohesive zone response for the FEM calculations.

Fig. 9(a) and (b) compare FEM simulations with the beam model in terms of the ratio $\Gamma_{0,\mathrm{FEM}}/\Gamma_{0,\mathrm{Beam}}$ for a peak stress $\sigma_\mathrm{p}/\sigma_0 = 1$, $D/h = 1.5$, different hardening exponents n and $\sigma_0/E = 0.001$ (a) and 0.01 (b). The figures show that for given values of n and σ_0/E, the beam model always underestimates the bond toughness. If the bond is characterized by a peak stress smaller than 1, it can be inferred from Fig. 5 that for a given radius of curvature R, the corresponding $\Gamma_{0,\mathrm{FEM}}$ will be larger. $\Gamma_{0,\mathrm{Beam}}$ is of course independent of the peak stress, and for a given R the ratio $\Gamma_{0,\mathrm{Beam}}/\Gamma_{0,\mathrm{FEM}}$ will be smaller with lower peak stresses leading to higher discrepancies. One possible reason for this discrepancy is that a decrease of the peak stress tends to increase the departure from the built-in beam assumption and increases the "root rotation" effects at the crack tip (Williams and Hadavinia, 2002), thus invalidating the approximation made with the beam bending model.

Fig. 10 shows that the agreement between the beam model and the numerical calculations is better for large wedge thickness D/h. This also agrees with the argument of Yang et al. (1999) that a thicker wedge leads to smaller shear stress and thus reduces the discrepancy with the beam model that neglects shear stresses.

For the range of values studied in this work, the beam formulation almost never overestimates the value of the bond toughness (except large D/h, low $\sigma_\mathrm{p}/\sigma_0$). The beam model is thus conservative in most cases. Figs. 9 and 10 can be used to correct the beam model formula, by interpolating between results if necessary.

4.2. Identification of the cohesive zone parameters

The analysis of the wedge-peel test proposed in this paper can be used for experimental evaluation of the adhesive bond toughness Γ_0 and peak cohesive strength σ_p when the adherents deform plastically during

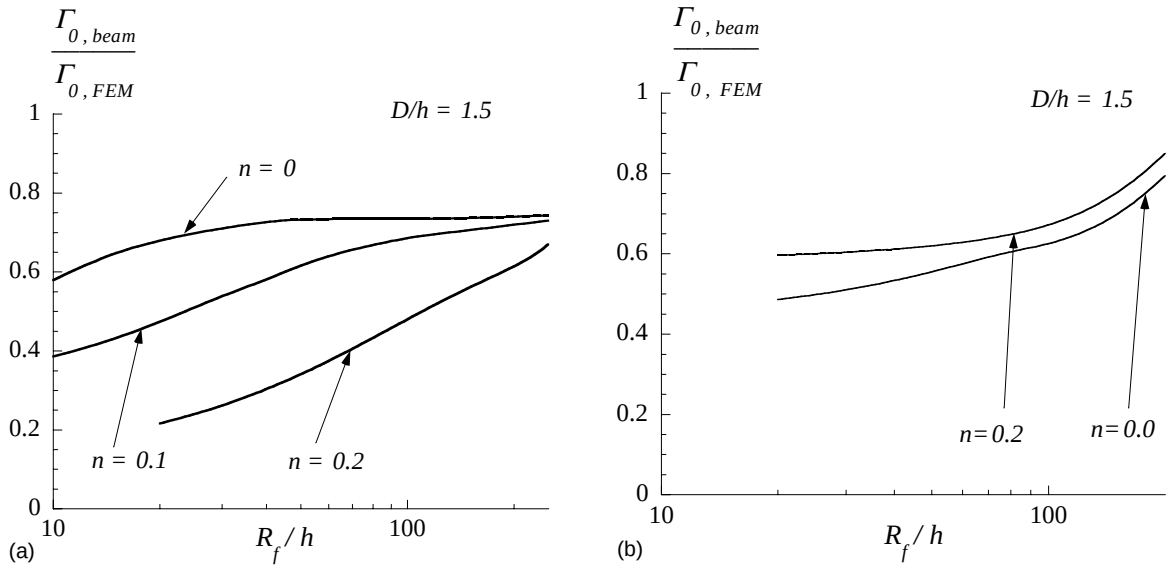

Fig. 9. (a) Comparison of the analytical and FEM predictions of the bond toughness for various R_f/h values with $\sigma_0/E = 0.001$ and $\sigma_p/\sigma_0 = 1.0$. (b) Comparison of the analytical and FEM predictions of the bond toughness for various R_f/h values with $\sigma_0/E = 0.01$ and $\sigma_p/\sigma_0 = 1.0$.

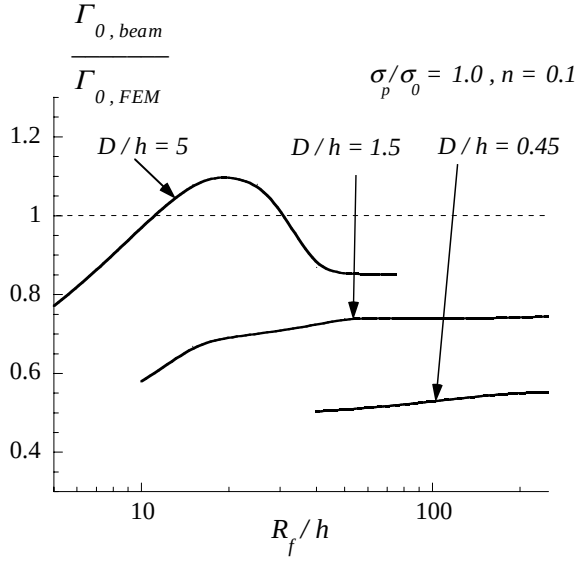

Fig. 10. Comparison of the analytical and FEM predictions of the bond toughness for various R_f/h and D/h values and for $\sigma_0/E = 0.001$.

debonding. Plastic deformations lead to a permanent curvature of the substrates R_f/h that can be measured after completion of the test, and the crack length can also be monitored during the test.

Chiang and Chai (1994), Daghyani et al. (1995), Yang et al. (1999) and Kafkalidis et al. (2000) have calibrated Γ_0 based on the measurement of the radius of curvature, while σ_p was evaluated independently using a finite element model for calculating the amplitude of traction forces in an adhesive layer. The procedure to calculate these traction forces follows a method proposed by Daghyani et al. (1995). In their approach, the adhesive layer is modeled by isotropic plasticity (i.e. J_2 flow theory). In the present paper, two calibration methods of the cohesive parameters are proposed based on two independent experimental measurements. Two pieces of experimental information are required, either the crack length and the average radius of curvature, or two radii of curvature obtained from two tests performed on substrates with different thickness h, or different mechanical properties (σ_0/E and n).

Fig. 11(a) illustrates the calibration method based on the measurement of the crack length and radius of curvature (i.e. a/h and R/h). An horizontal line is drawn at the level of the measured radius of curvature R/h. The intersection with the constant crack length curve that corresponds to the experimental value of a/h directly gives Γ_0 on the x-axis, while the peak stress has to be evaluated by interpolating between the "constant σ_p" curves. Only one test is required with this method. However, the experimental determination of the current steady state crack length is more difficult and less accurate than the measurement of the radius of curvature.

The calibration method based on the measurement of two radii of curvature for two different substrate thicknesses is illustrated on Fig. 11(b). The idea is to find the curve for which two abscissa values $\Gamma_0/\sigma_0 h_1$ and $\Gamma_0/\sigma_0 h_2$ are such that the ratio h_2/h_1 corresponds to the measured value. On a logarithmic scale, this procedure is quite straightforward since the ratio h_2/h_1 corresponds to a constant spacing along the x-axis. Care must be taken in selecting adherents having exactly the same surface characteristics and mechanical properties (e.g. by machining the plates from the same bulk material). If the mechanical properties of the adherents of thickness h_1 and h_2 are different, as for instance due to a different degree of rolling, the calibration must be performed with the data corresponding to the relevant σ_0/E and n values for each thickness.

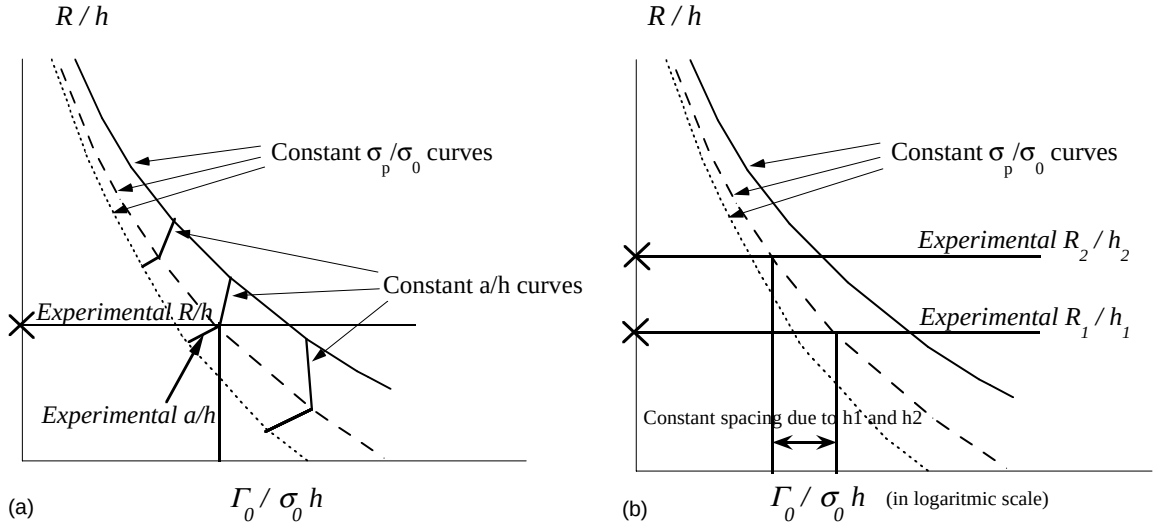

Fig. 11. (a) First calibration method of the cohesive zone parameters σ_p/σ_0 and $\Gamma_0/\sigma_0 h$ using the radius of curvature and crack length measured on a single specimen (schematic representation of the variation of R/h and a/h with $\Gamma_0/\sigma_0 h$). (b) Second calibration method of the cohesive zone parameters σ_p/σ_0 and $\Gamma_0/\sigma_0 h$ using the radii of curvature of two tests performed on two different systems with adherent thickness h_1 and h_2 (schematic representation of the variation of R/h and a/h with $\Gamma_0/\sigma_0 h$).

It is important to emphasize that the measurement of the radius of curvature after completion of the test is much easier to perform than a continuous measurement of the crack length. Thus, if substrates of different thicknesses are available, we recommend the technique using two radii of curvature. Note finally that a third calibration method can be envisioned based on the measurement of two radii of curvature with two different wedge heights. The advantage of this method is that the same adherents can be used. However, careful analysis of Fig. 7 shows that this method is not sufficiently precise, i.e. small errors in the measurement of the radii of curvature will lead to large uncertainties in the identification of Γ_0 and σ_p.

4.3. Optimization of the test

As mentioned previously, some degree of freedom exists for selecting the properties of the adherents that will allow for the most accurate experimental calibration. Of course, freedom in the choice of the substrate exists only when failure is cohesive (i.e. within the adhesive layer). In that case, the test measures the fracture properties of the adhesive layer in a constrained stress state that predominantly depends on the nature and thickness of the bond. When failure is adhesive (i.e. along the interface), the nature of the surface (in terms of treatment, roughness, and chemistry) is important and only the substrate thickness can be modified. Recall that the first rule with the wedge-peel test is to guarantee significant plasticity in the adherents. In fact, all of the figures presented in this paper show that the radius of curvature and crack length are more sensitive to the level of peak stress for small radii of curvature, i.e. for large degree of plastic yielding in the arms, than otherwise. The determination of bond toughness is slightly less sensitive to peak stress for smaller radii than for large radii.

For the method based on the measurement of two radii of curvature with two different adherent thicknesses, Fig. 11(b) shows that the quality of the calibration depends on the differences between the slopes of the R/h versus $\Gamma_0/\sigma_0 h$ curves corresponding to different peak stress. In other words, if the curves of Fig. 11(b) where parallel lines, the calibration would give an infinite number of solutions. The best compromise is found for low values of σ_0/E and, less importantly, low strain-hardening exponent n (e.g. a regular interstitial free steel with $\sigma_0/E = 0.001$).

Concerning the sensitivity of the method based on the measurement of the radius of curvature and crack length using a single test, Fig. 11(a) indicates that the best situation is encountered when the constant crack length lines are as close to vertical as possible. Critical analysis of Fig. 5(a)–(c) shows that the best choice for calibrating both the bond toughness and the peak stress is for high values of n and σ_0/E (e.g. an underaged aluminum of the 7XXX Series or a stainless steel will have these characteristics). Again, a compromise has to be found in the choice of the most suitable adherent materials.

Finally, Fig. 7 shows that a small wedge thickness is slightly better for both methods of calibration. However for a given adherent thickness, a thicker wedge gives rise to larger crack lengths, which are more easily measured.

5. Conclusion

A systematic study of the wedge-peel test has been performed using a steady state finite element method with the adhesive layer represented by a cohesive zone. The cohesive zone is characterized by an intrinsic toughness Γ_0 and a maximum strength σ_p. The adherents are modeled by J_2 flow theory. In particular, we have studied the influence of

(i) the adherent mechanical properties σ_0, E and n,
(ii) the adhesive fracture properties Γ_0 and σ_p,
(iii) the wedge height and the adherent thickness,

on test parameters that can be measured in an experiment. These parameters are

(i) the permanent radius of curvature of the adherents, and
(ii) the steady state crack length.

Two new calibration methods have been proposed for converting experimental data into cohesive zone properties. One method makes use of the measured crack length during testing and the measured radius of curvature of the deformed substrates. The other method uses the measured radii of curvature from tests performed on assemblies made of substrates having different thicknesses. Owing to the large range of parameters investigated, the results presented in this paper can be used to infer the bond toughness and strength of the adhesive layer for most assemblies.

An improved beam solution for the energy release rate incorporating the elastic unloading effects of the adherents has been proposed and assessed by comparison with the results of the steady-state numerical model. In particular, it has been shown that, in comparison to the steady-state numerical solution, the beam model performs best for thick wedges and when the adhesive layer has a high peak stress. In most circumstances accounting for elastic unloading of the adherents leads to a significant change in the predicted bond toughness. The results of this paper allow for the estimation of the error made with the beam model when inferring bond toughness.

Acknowledgements

The authors wish to express their appreciation to Prof. A.J. Kinloch (Imperial College, UK) and Dr. J.-Y. Sener (R&D Cockerill Sambre, Arcelor Group) for stimulating discussions. The financial support by the Research and Development Centre of Cockerill Sambre, Arcelor Group, and by the Walloon Region under grant FIRST-Doctorat 991/4161 is gratefully acknowledged.

References

ABAQUS Version 5.8, 1997. User's Manual. Hibbit, Karlsson and Sorensen, Providence, RI.

Chiang, M.Y.M., Chai, H., 1994. Plastic deformation analysis of cracked adhesive bonds loaded in shear. International Journal of Solids and Structures 31, 2477–2490.

Cognard, J., 2000. Science et technologie du collage. Presses Polytechniques et Universitaires, Romandes, Lausanne, Switzerland.

Daghyani, H.R., Ye, L., Mai, Y., 1995. Mode-I fracture behaviour of adhesive joints. Part II. Stress analysis and constraint parameters. Journal of Adhesion 53, 163–172.

Dean, R.H., Hutchinson, J.W., 1980. Quasi-static steady crack growth in small-scale yielding. In: Fracture Mechanics: 12th Conference, ASTM STP 700, American Society for Testing and Materials, pp. 383–405.

Ferracin, T., Pardoen, T., Sener, J., Delannay, F., 2000. Predictive fracture model for adhesively bonded joints failing with extensive plastic yielding. In: Miannay, D., Costa, P., François, D., Pineau, A. (Eds.), Proceedings of EUROMAT 2000, Advances in Mechanical Behaviour, Plasticity and Damage, Elsevier, Vol. 1, pp. 133–138.

Gaudenzi, P., Bathe, K.J., 1995. An iterative finite element procedure for the analysis of piezoelectric continua. Journal of Intelligent Material Systems And Structures 6, 266–273.

Hutchinson, J.W., Evans, A.G., 2000. Mechanics of materials: top–down approaches to fracture. Acta Materialia 48, 125–135.

Kafkalidis, M.S., Thouless, M.D., Yang, Q.D., Ward, M.S., 2000. Deformation and fracture of an adhesive layer constrained by plastically-deforming adherends. Journal of Adhesion Science and Technology 14, 1593–1607.

Kim, K.S., Aravas, N., 1988. Elastoplastic analysis of the peel test. International Journal of Solids and Structures 24, 417–435.

Kim, K.S., Kim, J., 1988. Elastoplastic analysis of the peel test for thin film adhesion. Journal of Engineering Materials and Technology 110, 266–273.

Landis, C.M., Pardoen, T., Hutchinson, J.W., 2000. Crack velocity dependent toughness in rate dependent material. Mechanics of Materials 32, 663–678.

Mohammed, I., Liechti, K.M., 2000. Cohesive zone modelling of crack nucleation in mixed-mode interfacial corners. Journal of the Mechanics and Physics of Solids 48, 735–764.

Needleman, A., 1987. A continuum model for void crack nucleation by inclusion debonding. Journal of Applied Mechanics 54, 525–531.

Sener, J., 1998. Ph.D. Thesis, Université catholique de Louvain, Belgium.

Thouless, M.D., Adams, J.L., Kafkalidis, M.S., Ward, S.M., Dickie, R.A., Westerbeek, G.L., 1998. Determining the toughness of plastically deforming joints. Journal of Materials Science 33, 189–197.

Tvergaard, V., Hutchinson, J.W., 1992. The relation between crack growth resistance and fracture process parameters in elastic-plastic solids. Journal of the Mechanics and Physics of Solids 40, 1337–1397.

Tvergaard, V., Hutchinson, J.W., 1994. Toughness of an interface along a thin ductile layer joining elastic solids. Philosophical Magazine A 70, 641–656.

Tvergaard, V., Hutchinson, J.W., 1996. On the toughness of ductile adhesive joints. Journal of the Mechanics and Physics of Solids 44, 789–800.

Williams, J.G., Hadavinia, H., 2002. Analytical solutions for cohesive zone models. Journal of the Mechanics and Physics of Solids 50, 809–825.

Wei, Y., Hutchinson, J.W., 1997. Interface strength, work of adhesion and plasticity in the peel test. International Journal of Fracture 93, 315–333.

Yang, Q.D., Thouless, M.D., Ward, S.M., 1999. Numerical simulation of adhesively-bonded beams failing with extensive plastic deformation. Journal of the Mechanics and Physics of Solids 47, 1337–1353.